Tao and Zhang
EURASIP Journal on Advances in Signal Processing (2024) 2024:89
https://doi.org/10.1186/s13634-024-01184-6

EURASIP Journal on Advances in Signal Processing

RESEARCH Open Access

Synergistic optimization strategy for beamforming and power allocation in dual-functional radar-communication systems

Jie Tao[1] and Zhenkai Zhang[1*]

*Correspondence:
zhangzhenkai@just.edu.cn

[1] Ocean College, Jiangsu University of Science and Technology, Zhenjiang 212000, Jiangsu, China

Abstract

The dual-functional radar-communication (DFRC) integrated system presents an ideal solution to address the challenge of spectrum resource congestion in future networks. This paper explores an adaptive power allocation technique based on beamforming to enhance the word error probability (WEP) performance of the DFRC system. Initially, a joint optimization model is developed to minimize the WEP while adhering to constraints on radar signal-to-interference-noise ratio (SINR), peak-to-average-power ratio, sidelobe level, and total transmit power. This model incorporates dual-function transmit beam, radar, and communication receive beam patterns. Subsequently, the proposed subproblem convex relaxation alternating update (SCRAU) algorithm is introduced to achieve a locally optimal solution for multi-carrier power allocation. This algorithm decomposes the original non-convex optimization problem into three sub-problems with lower complexity and iteratively optimizes them. Simulation experiments validate that the SCRAU algorithm can simultaneously fulfill radar and communication functions. The SCRAU algorithm demonstrates superior WEP performance compared to current advanced algorithms.

Keywords: Dual-functional radar-communication integrated system, Word error probability, Beamforming, Adaptive power allocation

1 Introduction

The advancement of 5G and the anticipated development of 6G technologies are escalating the demand for wireless spectrum within the global communication industry. To tap into additional spectrum resources, communication spectrum is being extended to higher frequency bands, leading to overlaps with radar spectrum [1, 2]. The dual-functional radar-communication (DFRC) integrated system, which achieves both radar and communication functions concurrently by utilizing shared hardware and spectrum resources, is considered a paradigm for the next generation of wireless systems and networks [3–5].

Currently, the predominant dual-function implementation schemes involve fast-time modulation for information embedding (IE) and the sidelobe control information embedding (SCIE) scheme [6]. In the DFRC integrated system, the primary drawback of fast information embedding schemes lies in the potential for inefficient bandwidth utilization, increased system complexity, and adverse impacts on communication performance [7, 8]. Conversely, the SCIE scheme in the DFRC integrated system offers a significant advantage in reducing interference, particularly in mitigating the interference from the radar system on the communication component. This contributes to enhancing the performance of the communication system, ensuring the reliability and stability of the communication link [9].

The SCIE scheme comes in various forms, including amplitude modulation (AM) [10], phase modulation (PM) [11] and quadrature amplitude modulation (QAM) [6]. A general framework for information embedding in frequency-hopped (FH) multiple-input-multiple-output (MIMO) DFRC system is introduced in [10]. A unified formula is defined to accommodate various existing modulation methods. The proposed hybrid modulation strategy significantly increases the data rate, but the scheme still has obvious defects in range sidelobe suppression and target detection. In [11], an adaptive DFRC system based on PM iteratively updates target scene parameters by learning from the radar scene at the receiver and dynamically reallocating transmit power. The goal is to adapt to the time-varying characteristics of radar targets and surroundings. A two-part waveform optimization method is proposed that improves target detection without affecting communication function. The optimization problem of DFRC transmit beamforming and receive beamforming is studied in [12]. The alternating direction sequential relaxation programming (ADSRP) algorithm is proposed, optimizing the detection performance of DFRC while simultaneously achieving the dual functions. In the integrated radar and communication system discussed in [13], an orthogonal frequency division multiplexing (OFDM) integrated signal with QAM is employed. To address the challenge of high peak-to-average power ratio (PAPR), an active constellation expansion algorithm is applied to control the PAPR of the integrated signal. This algorithm enhances target detection performance with minimal impact on the word error probability (WEP).

WEP measures the proportion of incorrectly interpreted words at the communication receiving end. A lower WEP indicates fewer data misinterpretations, helping to reduce the need for redundant information, improve system efficiency, and ensure better communication quality under various conditions [12]. PAPR has significant implications for the integration of radar and communication systems. Higher PAPR may lead to nonlinear distortions in power amplifiers, impacting the system's dynamic range [14]. In DFRC integrated systems, optimizing PAPR handling is crucial for system performance, reliability, flexibility, and adaptability to various communication environments. Optimizing power allocation enables efficient system operation, enhances communication reliability, minimizes overall energy consumption, and ensures stable system performance in complex environments [15]. Meanwhile, precise control of beamforming can further minimize radiation in non-target directions, reducing additional energy consumption. By synergistically optimizing beamforming and power allocation, the DFRC system can achieve better signal transmission and target detection performance, and improve the overall effectiveness of the system.

Increasing transmit power can improve radar SINR and communication WEP, but blindly increasing transmit power may consume resources and increase the risk of interception [16]. For the current research on multi-carrier power allocation in DFRC systems, the problem of optimizing communication WEP while considering total transmit power, PAPR and SINR is still not sufficiently concerned. To address this problem, we propose a multi-carrier power allocation problem for DFRC signals based on beamforming with sidelobe control information embedded in it. To ensure the Quality of Server (QoS), we comprehensively investigate transmit/receive beamforming in DFRC integrated systems. Since DFRC systems share transmission signals and equipment, the radar and communication performance are highly coupled. Relying only on radar or communication channel states for power allocation can severely degrade performance. Therefore, limited power allocation while realizing radar and communication functions has become an urgent problem.

This paper makes the following key contributions:

(1) Beamforming-Based Multi-Carrier Power Allocation: We introduce a beamforming-based approach to present a multi-carrier power allocation problem for integrated radar-communication signals. The objective is to minimize the word error probability (WEP) while considering constraints on radar signal-to-interference-noise ratio (SINR), sidelobe level (SLL), peak-to-average-power ratio (PAPR), and total transmit power.
(2) SCRAU Algorithm for Non-convex Optimization: To address the non-convex optimization problem, we propose the subproblem convex relaxation alternating update (SCRAU) algorithm. This algorithm decomposes the original non-convex problem into three sub-problems, achieving a locally optimal solution through alternating iterative optimization.

The paper is structured in the following manner: Section II introduces the system model and signal model; Section III elucidates the proposed algorithm; Section IV provides simulation results and analysis, and Section V presents the conclusions.

Notations: $(\cdot)^T$,$(\cdot)^\dagger$,$(\cdot)^*$,$|\cdot|$,$\|\cdot\|$,$E\{\cdot\}$,C,$C^{M\times 1}$,$C^{M\times M}$ and $I^{M\times M}$ denote transpose, conjugate transpose, conjugate, absolute value, the Euclidean norm, average value, complex ensemble, the set of $M \times 1$ vectors with complex entries, the set of $M \times M$ matrices with complex entries, and $M \times M$ identity matrix, respectively. $\mathcal{CN}(\cdot,\cdot)$ denotes the complex Gaussian distribution. Re$\{\cdot\}$ denotes the real part of the number in parentheses.

2 System model and signal model

Figure 1 illustrates the DFRC integrated system, which consists of dual-function transmitting co-located array, communication receiving array and radar receiving array. The dual-function transmitting co-located array contains M_T array elements, and the radar receiving array contains $M_{R,r}$ array elements, and communication receiving array contains $M_{R,c}$ array elements. The integrated signals transmitted by the dual-function transmitting array can realize both radar and communication functions. We consider the scenario where all arrays are assumed to be uniform linear arrays, and the spacing between array elements is set to half the wavelength. The radar and communication

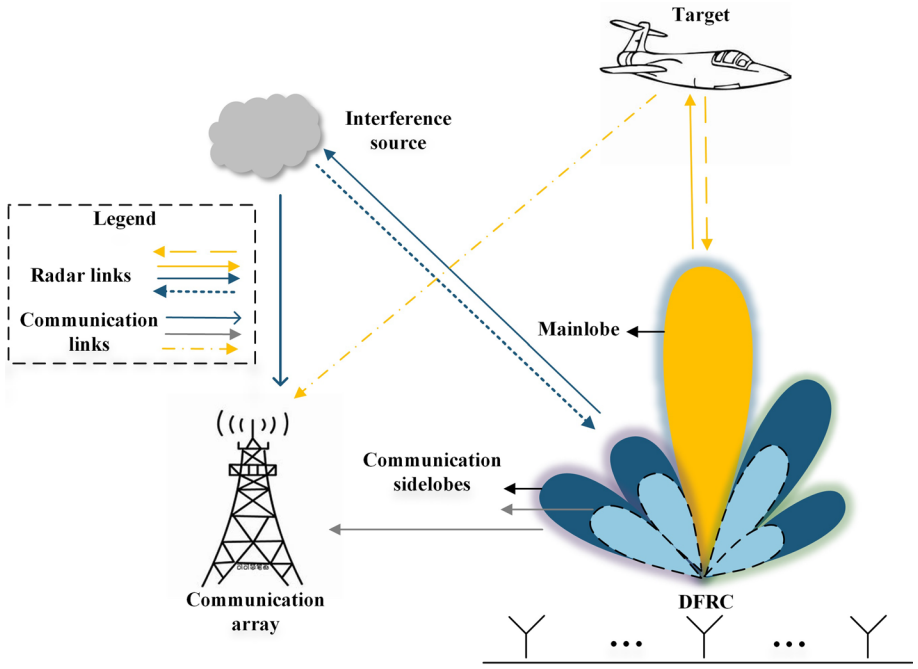

Fig. 1 DFRC integrated system

receiving arrays have the same number of array elements, that is $M_{R,r} = M_{R,c} = M_T$. In this model, the radar transmitting and the receiving arrays are positioned in close proximity. Looking from the viewpoint of the target in Fig. 1, the DFRC transmitting array and the radar receiving array are assumed to be positioned at the same angle. Assuming that we have information about each angle and the channel state information (CSI) for both the radar and communication [12].

$\{s_n\}_{n=1}^{N}$ is defined as an integrated multi-carrier signal with N subcarriers. Let Δf be the frequency interval of the subcarriers and assume that Δf is large enough, then the subcarriers are independent of each other. The power of the $n{-}th$ subcarrier is $E\{|s_n|^2\} = P_n$. In the DFRC integrated system, the radar and communication functions are implemented by the s_n of the dual-function transmitter. The main lobe of the beam pointing to the detection target is used to detect the information of the target, and the sidelobe of the beam pointing to the communication user transmits the communication symbol. Radar performance is affected by the source of interference, and from the perspective of the communication, the reflected signal from both the target and the interference source can affect the communication performance.

$\boldsymbol{q}_n = [q_{1,n}, q_{2,,n}, ..., q_{M_T,n}]^{\dagger} \in C^{M_T \times 1}$ is defined as the transmit beamforming vector of $M_T \times 1$ on the $n{-}th$ subcarrier, where $\|\boldsymbol{q}_n\| = 1$. At the dual-function transmitter, s_n and $\boldsymbol{q}_n$ are multiplied to obtain the integrated transmission signal $\boldsymbol{q}_n s_n$ of M_T elements on the $n{-}th$ subcarrier. Target detection is achieved through the analysis of echo signals received by the radar receiving array. Simultaneously, the communication receiving array processes the received signals to facilitate the transmission of information.

$\boldsymbol{v}_n = [v_{1,n}, v_{2,n}..., v_{M_R,n}]^{\dagger} \in C^{M_R \times 1}$ is defined as the radar receive beamforming vector on the $n{-}th$ subcarrier which is of size $M_R \times 1$. Assume that the channel between the dual-function transmitting co-located array and the target (the interference source)

is $H \in C^{M_T \times M_T}(H_I \in C^{M_T \times M_T})$, respectively. The target and the interference source are located at angles ω_0 and ω_1, respectively. Then the received signal on the $n-th$ subcarrier at the radar receiving array is

$$y_{r,n} = \boldsymbol{v}_n^{\dagger}(\boldsymbol{H}_n + \boldsymbol{H}_{I,n})\boldsymbol{q}_n s_n + \boldsymbol{v}_n^{\dagger}\varpi_{r,n} \tag{1}$$

where $\boldsymbol{H}_n = a_{0,n}\boldsymbol{\beta}(\omega_0)\boldsymbol{\alpha}(\omega_0)^T$ and $\boldsymbol{H}_{I,n} = a_{1,n}\boldsymbol{\beta}(\omega_1)\boldsymbol{\alpha}(\omega_1)^T.\boldsymbol{\alpha}(\omega) \in C^{M_T}$ and $\boldsymbol{\beta}(\omega) \in C^{M_R}$ are the transmitting and receiving steering vectors pointing to the angle ω, respectively. $a_{0,n} \in C$ and $a_{1,n} \in C$ are the channel coefficients on the corresponding $n-th$ subcarrier and obey complex Gaussian distributions $\mathcal{CN}\left(0,\ \sigma_{a,0,n}^2\right)$ and $\mathcal{CN}\left(0,\ \sigma_{a,1,n}^2\right)$, respectively. $\varpi_{r,n} \in C^{M_R \times 1}$ represents the noise vector of the radar on the $n-th$ subcarrier and obeys Gaussian distribution $\mathcal{CN}\left(0, \sigma_{r,n}^2 \boldsymbol{I}_{M_R \times M_R}\right)$.

Assume that $\boldsymbol{u}_n = \boldsymbol{q}_n s_n$, the received signal $y_{r,n}$ is filtered by $\boldsymbol{v}_n$ to improve the radar SINR of the $n-th$ subcarrier at the radar receiving array.

$$SINR_{r,n} = \frac{\sigma_{a,0,n}^2 \left|\boldsymbol{v}_n^{\dagger}\boldsymbol{H}_n\boldsymbol{u}_n\right|^2}{\boldsymbol{v}_n^{\dagger}\boldsymbol{\psi}_n\boldsymbol{v}_n + \sigma_{r,n}^2\boldsymbol{v}_n^{\dagger}\boldsymbol{v}_n} \tag{2}$$

where $\boldsymbol{\psi}_n = E\left\{\boldsymbol{H}_{I,n}\boldsymbol{u}_n\boldsymbol{u}_n^{\dagger}\boldsymbol{H}_{I,n}^{\dagger}\right\}$.

Assume the communication receiving array is positioned at azimuth angle ∂, the baseband communication transmission signal on the $n-th$ subcarrier is

$$\boldsymbol{d}_n = \alpha^T(\partial)\boldsymbol{u}_n s_n, (l = 1, ..., L, n = 1, ..., N) \tag{3}$$

where each value of $\boldsymbol{d}_n$ corresponds to only one particular communication symbol. In order to transmit $\log_2(L)$-bit symbols (one pulse duration) on each subcarrier, L $\boldsymbol{d}_n$ different transmit beams need to be designed and stored in the code word dictionary $\mathcal{D} = \left\{\boldsymbol{d}_{1,n}, ..., \boldsymbol{d}_{L,n}\right\}$. The transmission of communication symbols is achieved by controlling the amplitude of the expression (3), i.e., the sidelobe level of the transmitted beam in the direction of the azimuth angle. Therefore, during the duration of the pulse, a $\boldsymbol{d}_{l,n}$ is selected from $\mathcal{D} = \left\{\boldsymbol{d}_{1,n}, ..., \boldsymbol{d}_{L,n}\right\}$. At the communication receiving end, the corresponding symbol is determined by judging the $\boldsymbol{d}_{l,n}$, and then the symbol transmission is completed.

$\boldsymbol{w}_n = \left[w_{1,n}, w_{2,n}, ..., w_{M_R,n}\right]^{\dagger} \in C^{M_R \times 1}$ is defined as the communication receive beamforming vector on the $n-th$ subcarrier, which is of size $M_R \times 1$.The received signal at the communication receiving array comprises both the desired signal and interference signal. The desired signal comes from the dual-function transmitting array. The interference signal comes from the reflection of the target or from the reflection of the interference source. The received signal on the $n-th$ subcarrier at the communication receiving array is

$$y_{c,n} = \boldsymbol{w}_n^{\dagger}(\gamma_n\boldsymbol{\beta}(\partial^*)\boldsymbol{\alpha}(\partial))^T + b_{0,n}\boldsymbol{\beta}(\vartheta_0)\boldsymbol{\alpha}(\omega_0)^T + b_{1,n}\boldsymbol{\beta}(\vartheta_1)\boldsymbol{\alpha}(\omega_1)^T)\boldsymbol{q}_n s_n + \boldsymbol{w}_n^{\dagger}\varpi_{c,n} \tag{4}$$

where ∂^*,ϑ_0 and ϑ_1 are the angles of arrival of the transmitted signal (reception angle of the communication array), the angle of the desired communication signal and the angle of the communication interference signal, respectively. γ_n is the communication channel coefficient on the $n-th$ subcarrier and obeys $\mathcal{CN}\left(0,\ \sigma_{\gamma,n}^2\right)$. $b_{0,n} \in C(b_{1,n} \in C)$ is the channel coefficient of the $n-th$ subcarrier from the transmitter to the reflectors (target

and interference source) and then to the communication user.$b_{0,n} \in C$ ($b_{1,n} \in C$) obeys $\mathcal{CN}\left(0,\ \sigma_{b,0,n}^2\right)(\mathcal{CN}\left(0,\ \sigma_{b,1,n}^2\right))$. $\varpi_{c,n} \in C^{M_R \times 1}$ is the communication noise vector on the $n-th$ subcarrier and obeys Gaussian distribution $\mathcal{CN}\left(0,\ \sigma_{c,n}^2 \boldsymbol{I}_{M_R \times M_R}\right)$.

The received signal $y_{c,n}$ is filtered by $\boldsymbol{w}_n$ to improve the communication SINR on the $n-th$ subcarrier at the communication receiving array.

$$SINR_{c,n} = \frac{\sigma_{\gamma,n}^2 \left|\boldsymbol{w}_n^{\dagger} \boldsymbol{\beta}(\partial^*)\right|^2}{\boldsymbol{w}_n^{\dagger} \mathcal{M}_n \boldsymbol{w}_n + \sigma_{c,n}^2 \boldsymbol{w}_n^{\dagger} \boldsymbol{w}_n} \tag{5}$$

where $\mathcal{M}_n = E\left\{\boldsymbol{f}_n \boldsymbol{u}_n \boldsymbol{u}_n^{\dagger} \boldsymbol{f}_n^{\dagger}\right\}$ and $\boldsymbol{f}_n = a_{0,k} \boldsymbol{\beta}(\vartheta_0) \boldsymbol{\alpha}(\omega_0)^T + a_{1,k} \boldsymbol{\beta}(\vartheta_1) \boldsymbol{\alpha}(\omega_1)^T$.

The amplitude of the transmitted sidelobes for each pulse is selected from a predesigned codebook $\boldsymbol{d}_l = \left(d_{l,1}, ..., d_{l,N}\right)^T \in C^N$. This codebook consists of L code words of length N, i.e., $\mathcal{D} = \{\boldsymbol{d}_1, ..., \boldsymbol{d}_L\}$. The identification of the communication symbol for the communication user is based on the comparison of the amplitude of the received signal $\left|y_{c,n}\right|$ on the $n-th$ subcarrier with $L-1$ thresholds. We assume that $\boldsymbol{d}_{\ell}$ is the communication transmit symbol, during the pulse duration, the expression for the communication WEP is [17].

$$W_l = \left\{ \frac{1}{2}(L-1) \exp(-\min_{s \neq l} \sum_{n=1}^{N} \frac{\sigma_{\gamma,n}^2 \left|\boldsymbol{w}_n^{\dagger} \boldsymbol{\beta}(\partial^*)\right|^2 \left|\boldsymbol{d}_{l,n} - \boldsymbol{d}_{s,n}\right|^2}{4(\boldsymbol{w}_n^{\dagger} \mathcal{M}_n \boldsymbol{w}_n + \sigma_{c,n}^2 \boldsymbol{w}_n^{\dagger} \boldsymbol{w}_n)}) \right\} \tag{6}$$

where $\boldsymbol{d}_{l,n}$ is a code word different from $\boldsymbol{d}_{s,n}$.

3 Multi-carrier power allocation algorithm for integrated signals

The objective is to minimize WEP in a DFRC integrated system with beamforming, considering constraints on radar SINR, PAPR, and total transmit power. The multi-carrier power allocation scheme $\boldsymbol{P} = [\|\boldsymbol{u}_1\|^2, \|\boldsymbol{u}_2\|^2, ..., \|\boldsymbol{u}_N\|^2]^T$ can be derived through the optimization problem presented as follows [18]

$$\mathcal{P}: \ \arg\min_{\{\boldsymbol{u}_n, \boldsymbol{v}_n, \boldsymbol{w}_n\}} \left\{ \frac{1}{2}(L-1) \exp\left(-\min_{s \neq l} \sum_{n=1}^{N} \frac{\sigma_{r,n}^2 \left|\boldsymbol{w}_n^{\dagger} \boldsymbol{\beta}(\partial^*)\right|^2 \left|\boldsymbol{d}_{l,n} - \boldsymbol{d}_{s,n}\right|^2}{4(\boldsymbol{w}_n^{\dagger} \mathcal{M}_n \boldsymbol{w}_n + \sigma_{c,n}^2 \boldsymbol{w}_n^{\dagger} \boldsymbol{w}_n)} \right) \right\} \tag{7a}$$

$$s.t. \begin{cases} C1: \sum_{n=1}^{N} \dfrac{\left|\boldsymbol{v}_n^{\dagger} \boldsymbol{C}_n \boldsymbol{u}_n\right|^2}{\boldsymbol{v}_n^{\dagger} \boldsymbol{\Psi}_n \boldsymbol{v}_n + \sigma_{r,n}^2 \boldsymbol{v}_n^{\dagger} \boldsymbol{v}_n} \geq \Re \\ C2: \sum_{n=1}^{N} \|\boldsymbol{u}_n\|^2 \leq P_{tot} \\ C3: \boldsymbol{\alpha}^T(\partial) \boldsymbol{u}_n = \boldsymbol{d}_{\ell,n}, 1 \leq n \leq N, 1 \leq \ell \leq L \\ C4: PAPR \leq \delta_p \end{cases} \tag{7b}$$

where $C1$ indicates that the sum of radar SINR should not exceed $\Re$; $C2$ indicates that the transmit power cannot exceed P_{tot}; $C3$ controls the amplitude of the side flap pointing in azimuth to accomplish communication symbol transmission; $C4$ indicates that the PAPR cannot exceed δ_p. In addition, it can be seen from constraint $C3$ that in order to transmit $\log_2 L$ bit symbols/pulses, optimization problem (7) needs to be solved L times. The PAPR is denoted as [19]

$$PAPR = \frac{\max\limits_{n} \|\boldsymbol{u}_n\|^2}{\frac{1}{N}\sum\limits_{n=1}^{N} \|\boldsymbol{u}_n\|^2}, 1 \le n \le N \tag{8}$$

Since the optimization problem (7) is high-dimensional and non-convex, it is hard to solve the closed-form solution directly. Drawing inspiration from the algorithm introduced in [20, 21], the divisible structure of the objective function allows for its expression as follows:

$$\arg\min_{\{\boldsymbol{u}_n,\boldsymbol{v}_n,\boldsymbol{w}_n\}} WEP = \left(\arg\min_{\{\boldsymbol{u}_n\}} WEP, \arg\min_{\{\boldsymbol{v}_n\}} WEP, \arg\min_{\{\boldsymbol{w}_n\}} WEP\right) \tag{9}$$

To obtain a suboptimal solution of problem (9), i.e., $\{\boldsymbol{u}_n^*, \boldsymbol{v}_n^*, \boldsymbol{w}_n^*\}$, an iterative SCRAU algorithm is introduced, aiming to tackle the three low-complexity sub-problems. Let $\{\boldsymbol{u}_n^t, \boldsymbol{v}_n^t, \boldsymbol{w}_n^t\}$ denote the solution in the $t-th$ iteration, $t \ge 1$. Firstly, a feasible initial value $\{\boldsymbol{u}_n^0, \boldsymbol{v}_n^0, \boldsymbol{w}_n^0\}$ is set and then iteratively solve sub-problems $\boldsymbol{u}_n$,$\boldsymbol{v}_n$ and $\boldsymbol{w}_n$. To attain the solution by the $(t+1)-th$ iterative step, the following iterative optimization procedure is given:

(1) update $\boldsymbol{u}_n^{t+1}$ by fixing $\boldsymbol{v}_n^t$ and $\boldsymbol{w}_n^t$;
(2) update $\boldsymbol{v}_n^{t+1}$ by fixing $\boldsymbol{u}_n^{t+1}$ and $\boldsymbol{w}_n^t$;
(3) update $\boldsymbol{w}_n^{t+1}$ by fixing $\boldsymbol{u}_n^{t+1}$ and $\boldsymbol{v}_n^{t+1}$.

The iteration process stops when the difference between the optimization results in the $(t+1)-th$ iteration and the $t-th$ iteration is not more than ε.

$$\left\| W_l^{t+1}(\boldsymbol{u}_n, \boldsymbol{v}_n, \boldsymbol{w}_n) - W_l^t(\boldsymbol{u}_n, \boldsymbol{v}_n, \boldsymbol{w}_n) \right\| \le \varepsilon \tag{10}$$

where $W_l^t(\boldsymbol{u}_n, \boldsymbol{v}_n, \boldsymbol{w}_n)$ denotes the minimum value of WEP obtained in the $t-th$ iteration, and ε is a predefined constant used as the stopping criterion for iterations.

A. Radar Transmit Beamformer Update

When $\boldsymbol{v}_n^t$ and $\boldsymbol{w}_n^t$ are fixed to solve out $\boldsymbol{u}_n^{t+1}$, (7a) takes the following shape

$$W_l\left(\boldsymbol{u}_n^{t+1} \middle| \{\boldsymbol{v}_n^t, \boldsymbol{w}_n^t\}\right) = \frac{1}{2}(L-1)\exp\left(-\min_{s\ne l}\sum_{n=1}^{N} \frac{\sigma_{r,n}^2 \left|(\boldsymbol{w}_n^t)^\dagger \boldsymbol{\beta}(\partial^*)\right|^2 \left|\boldsymbol{d}_{l,n} - \boldsymbol{d}_{s,n}\right|^2}{4\left((\boldsymbol{w}_n^t)^\dagger \mathcal{M}_n \boldsymbol{w}_n^t + \sigma_{c,n}^2 (\boldsymbol{w}_n^t)^\dagger \boldsymbol{w}_n^t\right)}\right) \tag{11}$$

Therefore, when $\boldsymbol{v}_n^t$ and $\boldsymbol{w}_n^t$ are fixed, $\boldsymbol{u}_n^{t+1}$ can be obtained by solving $\mathcal{P}_1$.

$$\mathcal{P}_1: \left\{\boldsymbol{u}_n^{t+1}\right\} = \arg\min_{\{\boldsymbol{u}_n\}} \left\{\exp\left(-\min_{s\ne l}\sum_{n=1}^{N} \frac{\sigma_{r,n}^2 \left|(\boldsymbol{w}_n^t)^\dagger \boldsymbol{\beta}(\partial^*)\right|^2 \left|\boldsymbol{d}_{l,n} - \boldsymbol{d}_{s,n}\right|^2}{4\left((\boldsymbol{w}_n^t)^\dagger \mathcal{M}_n \boldsymbol{w}_n^t + \sigma_{c,n}^2 (\boldsymbol{w}_n^t)^\dagger \boldsymbol{w}_n^t\right)}\right)\right\}$$

$$s.t.\ C1, C2, C3, C4 \tag{12}$$

Because of the non-convexity of $C1$ and $C4$, the optimization problem (12) is non-convex. We can transform problem (12) into a relaxed convex problem and subsequently solve it.

1) Relaxation of the objective function in (12)

Since $SINR_{c,n}$ is non-convex in the objective function (12), we perform a convex transformation on $SINR_{c,n}$. Firstly, $SINR_{c,n}$ can be rewritten as

$$SINR_{c,n} = \frac{\boldsymbol{\zeta}_n^t}{\boldsymbol{u}_n^\dagger \boldsymbol{\mathcal{G}}_n^t \boldsymbol{u}_n + \xi_n^t} \tag{13}$$

where $\boldsymbol{\zeta}_n^t = \sigma_{r,n}^2 \left|(\boldsymbol{w}_n^t)^\dagger \boldsymbol{\beta}(\partial^*)\right|^2$, $\xi_n^t = \sigma_{c,n}^2 \left(\boldsymbol{w}_n^t\right)^\dagger \boldsymbol{w}_n^t$ and $\boldsymbol{\mathcal{G}}_n^t = \boldsymbol{f}_n^t \boldsymbol{w}_n^t \left(\boldsymbol{w}_n^t\right)^\dagger \left(\boldsymbol{f}_n^t\right)^\dagger$. In accordance with the linear approximation from the first-order Taylor series expansion [22]

$$1/x \geq 1/x^0 - 1/\left(x^0\right)^2 \left(x - x^0\right) \tag{14}$$

where the equation holds true when $x = x^0$. Subsequently, according to (14), it can be derived that

$$SINR_{c,n} \geq \boldsymbol{\zeta}_n^t \left[\frac{1}{\left(\boldsymbol{u}_n^t\right)^\dagger \boldsymbol{\mathcal{G}}_n^t \boldsymbol{u}_n^t + \xi_n^t} - \frac{\left(\boldsymbol{u}_n^t\right)^\dagger \boldsymbol{\mathcal{G}}_n^t \left(\boldsymbol{u}_n - \boldsymbol{u}_n^t\right)}{\left(\left(\boldsymbol{u}_n^t\right)^\dagger \boldsymbol{\mathcal{G}}_n^t \boldsymbol{u}_n^t + \xi_n^t\right)^2} \right] \tag{15}$$

where $\boldsymbol{u}_n^t$ denotes the transmit beam formation vector obtained in the previous iteration. The objective function (11) is equivalently replaced by (15), i.e.,

$$\exp\left\{ -\min_{s \neq l} \frac{\eta_l}{4} \sum_{n=1}^{N} \boldsymbol{\zeta}_n^t \left[\frac{1}{\left(\boldsymbol{u}_n^t\right)^\dagger \boldsymbol{\mathcal{G}}_n^t \boldsymbol{u}_n^t + \xi_n^t} - \frac{\left(\boldsymbol{u}_n^t\right)^\dagger \boldsymbol{\mathcal{G}}_n^t \left(\boldsymbol{u}_n - \boldsymbol{u}_n^t\right)}{\left(\left(\boldsymbol{u}_n^t\right)^\dagger \boldsymbol{\mathcal{G}}_n^t \boldsymbol{u}_n^t + \xi_n^t\right)^2} \right] \right\} \tag{16}$$

where $\eta_l = \left|\boldsymbol{d}_{l,n} - \boldsymbol{d}_{s,n}\right|^2$.

2) Relaxation of $C1$ in (12)

To solve out $\boldsymbol{u}_n^{t+1}$ by fixing $\boldsymbol{v}_n^t$ and $\boldsymbol{w}_n^t$, we rewrite $C1$ as

$$SINR_{r,n} = \sum_{n=1}^{N} \frac{\left|\left(\boldsymbol{v}_n^t\right)^\dagger \boldsymbol{H}_n \boldsymbol{u}_n\right|^2}{\left(\boldsymbol{v}_n^t\right)^\dagger \boldsymbol{\psi}_n \boldsymbol{v}_n^t + \sigma_{r,n}^2 \left(\boldsymbol{v}_n^t\right)^\dagger \boldsymbol{v}_n^t} = \sum_{n=1}^{N} \frac{\boldsymbol{u}_n^\dagger \left|\left(\boldsymbol{v}_n^t\right)^\dagger \boldsymbol{H}_n\right|^2 \boldsymbol{u}_n}{\boldsymbol{u}_n^\dagger \mathcal{T}_n^t \boldsymbol{u}_n + \sigma_{r,n}^2 \left(\boldsymbol{v}_n^t\right)^\dagger \boldsymbol{v}_n^t} \geq \Re \tag{17}$$

where $\mathcal{T}_n = E\left\{\boldsymbol{H}_{I,n} \boldsymbol{v}_n^t \left(\boldsymbol{v}_n^t\right)^\dagger \boldsymbol{H}_{I,n}^T\right\}$. The following Eq. (18) is obtained by shifting the terms left and right on both sides of the inequality.

$$\boldsymbol{u}_n^\dagger \left|\boldsymbol{v}_n^\dagger \boldsymbol{H}_n\right|^2 \boldsymbol{u}_n - \Re\left(\boldsymbol{u}_n^\dagger \mathcal{T}_n \boldsymbol{u}_n + \sigma_{r,n}^2 \boldsymbol{v}_n^\dagger \boldsymbol{v}_n\right) \geq 0 \tag{18}$$

3) Relaxation of $C4$ in (12)

From [19], constraint $C4$ can be recast as

$$\boldsymbol{u}_n^\dagger \mathcal{Q}_n \boldsymbol{u}_n - \frac{\delta_p}{N} \sum_{n=1}^{N} \boldsymbol{u}_n^\dagger \boldsymbol{u}_n \leq 0 \tag{19}$$

where

$$\mathcal{Q}_n(n_1,n_2)=\begin{cases}1,\ n_1=n\ and\ n_2=n\\ 0,\ otherwise\end{cases} \tag{20}$$

We use the first-order expansion condition to obtain

$$\boldsymbol{u}_n^{\dagger}\boldsymbol{u}_n \geq \left(\boldsymbol{u}_n^t\right)^{\dagger}\boldsymbol{u}_n^t + 2\mathrm{Re}\left\{\left(\boldsymbol{u}_n^t\right)^{\dagger}\boldsymbol{u}_n^t - \boldsymbol{u}_n^{\dagger}\boldsymbol{u}_n\right\} \tag{21}$$

According to (19) and (21), the constraint $C4$ can be equivalently replaced as

$$\boldsymbol{u}_n^{\dagger}\mathcal{Q}_n\boldsymbol{u}_n - \frac{\delta_p}{N}\times\sum_{n=1}^{N}\left(\left(\boldsymbol{u}_n^t\right)^{\dagger}\boldsymbol{u}_n^t + 2\mathrm{Re}\left\{\left(\boldsymbol{u}_n^t\right)^{\dagger}\boldsymbol{u}_n^t - \boldsymbol{u}_n^{\dagger}\boldsymbol{u}_n\right\}\right)\leq 0 \tag{22}$$

Problem (12) can be formulated as the relaxation problem presented below

$$\left\{\boldsymbol{u}_n^{t+1}\right\} = \arg\min_{\{\boldsymbol{u}_n\}}\exp\left\{-\min_{s\neq l}\frac{\eta_\ell}{4}\sum_{n=1}^{N}\zeta_n^t\left[\frac{1}{\left(\boldsymbol{u}_n^t\right)^{\dagger}\mathcal{G}_n^t\boldsymbol{u}_n^t+\xi_n^t} - \frac{\left(\boldsymbol{u}_n^t\right)^{\dagger}\mathcal{G}_n^t\left(\boldsymbol{u}_n-\boldsymbol{u}_n^t\right)}{\left(\left(\boldsymbol{u}_n^t\right)^{\dagger}\mathcal{G}_n^t\boldsymbol{u}_n^t+\xi_n^t\right)^2}\right]\right\}$$

$$s.t.\ (18), C2, C3, (22) \tag{23}$$

The convexity of the optimization problem (23) enables the acquisition of its optimal solution through the utilization of the CVX toolbox [23].

B. Radar Receive Beamformer Update

When $\boldsymbol{u}_n^{t+1}$ and $\boldsymbol{w}_n^t$ are fixed to solve out $\boldsymbol{v}_n^{t+1}$, $\boldsymbol{v}_n^{t+1}$ can be obtained by (24)

$$\left\{\nu_n^{t+1}\right\} = \arg\max_{\{\boldsymbol{v}_n\}}\frac{\left|\boldsymbol{v}_n^{\dagger}\boldsymbol{H}_n\boldsymbol{u}_n^{t+1}\right|^2}{\boldsymbol{v}_n^{\dagger}\boldsymbol{\psi}_n^{t+1}\boldsymbol{v}_n+\sigma_{r,n}^2\boldsymbol{v}_n^{\dagger}\boldsymbol{v}_n} = \arg\max_{\{\boldsymbol{v}_n\}}\frac{\left|\boldsymbol{v}_n^{\dagger}\boldsymbol{H}_n\boldsymbol{u}_n^{t+1}\right|^2}{\boldsymbol{v}_n^{\dagger}\left(\boldsymbol{\psi}_n^{t+1}+\sigma_{r,n}^2\boldsymbol{I}_{M_R\times M_R}\right)\boldsymbol{v}_n} \tag{24}$$

The optimization problem (24) can be equated to the minimum variance distortionless response (MVDR) beamforming problem [24]:

$$\mathcal{P}_2:\ \arg\min_{\{\boldsymbol{v}_n\}}\left[\boldsymbol{v}_n^{\dagger}\left(\boldsymbol{\psi}_n+\sigma_{r,n}^2\boldsymbol{I}_{M_R\times M_R}\right)\boldsymbol{v}_n\right]$$

$$s.t.\left|\boldsymbol{v}_n^{\dagger}\boldsymbol{C}_n\boldsymbol{u}_n^{t+1}\right| = 1 \tag{25}$$

Therefore, the local analytic solution of $\boldsymbol{v}_n^{t+1}$ is

$$\boldsymbol{v}_n^{t+1} = \frac{\left(\boldsymbol{\psi}_n^{t+1}+\sigma_{r,n}^2\boldsymbol{I}_{M_R\times M_R}\right)^{-1}\boldsymbol{H}_n\boldsymbol{u}_n^{t+1}}{\left(\boldsymbol{u}_n^{t+1}\right)^{\dagger}\boldsymbol{H}_n^T\left(\boldsymbol{\psi}_n^{t+1}+\sigma_{r,n}^2\boldsymbol{I}_{M_R\times M_R}\right)^{-1}\boldsymbol{H}_n\boldsymbol{u}_n^{t+1}} \tag{26}$$

C. Communication Receive Beamformer Update

When $\boldsymbol{u}_n^{t+1}$ and $\boldsymbol{v}_n^{t+1}$ are fixed to solve out $\boldsymbol{w}_n^{t+1}$, $\boldsymbol{w}_n^{t+1}$ can be obtained by (27)

$$\left\{\boldsymbol{w}_n^{t+1}\right\} = \arg\max_{\{\boldsymbol{w}_n\}}\frac{\sigma_{r,n}^2\left|\boldsymbol{w}_n^{\dagger}\boldsymbol{\beta}(\partial^*)\right|^2}{\boldsymbol{w}_n^{\dagger}\mathcal{M}_n^{t+1}\boldsymbol{w}_n+\sigma_{c,n}^2\boldsymbol{w}_n^{\dagger}\boldsymbol{w}_n} = \arg\max_{\{\boldsymbol{w}_n\}}\frac{\sigma_{r,n}^2\left|\boldsymbol{w}_n^{\dagger}\boldsymbol{\beta}(\partial^*)\right|^2}{\boldsymbol{w}_n^{\dagger}\left(\mathcal{M}_n^{t+1}+\sigma_{c,n}^2\boldsymbol{I}_{M_R\times M_R}\right)\boldsymbol{w}_n} \tag{27}$$

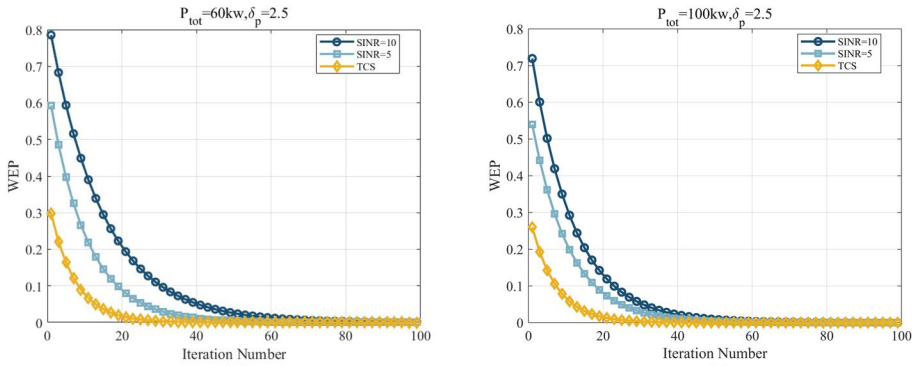

Fig. 2 Plot of WEP versus number of iterations at different conditions. **a** $P_{tot} = 60$ kw, $\delta_p = 2.5$, **b** $P_{tot} = 100$ kw, $\delta_p = 2.5$

The optimization problem (27) can be equated to the MVDR beamforming problem:

$$\mathcal{P}_3 : \arg\min_{\{\boldsymbol{w}_n\}} \left[\boldsymbol{w}_n^{\dagger}\left(\mathcal{M}_n^{t+1} + \sigma_{c,n}^2 \boldsymbol{I}_{M_R \times M_R}\right)\boldsymbol{w}_n\right]$$

$$s.t.\, \sigma_{r,n}^2 \left|\boldsymbol{w}_n^{\dagger}\boldsymbol{\beta}\left(\partial^*\right)\right| = 1 \tag{28}$$

Therefore, the local analytic solution of $\boldsymbol{w}_n^{t+1}$ is

$$\boldsymbol{w}_n^{t+1} = \frac{\left(\mathcal{M}_n^{t+1} + \sigma_{c,n}^2 \times \boldsymbol{I}_{M_C \times M_C}\right)^{-1}\boldsymbol{\beta}(\partial^*)}{\boldsymbol{\beta}(\partial^*)^{\dagger}\left(\mathcal{M}_n^{t+1} + \sigma_{c,n}^2 \times \boldsymbol{I}_{M_C \times M_C}\right)^{-1}\boldsymbol{\beta}(\partial^*)} \tag{29}$$

D. Algorithm Complexity and Convergence Analysis

1) Algorithm Complexity Analysis

The complexity of the proposed SCRAU is related to N, the dimension of $\boldsymbol{u}_n$,$\boldsymbol{v}_n$,$\boldsymbol{w}_n$ and the number of iterations. The relaxed convex problem (23) is solved using the interior point method (IPM) (via the CVX toolbox) during the $t-th$ iteration to get $\boldsymbol{u}_n^t$. Its computational complexity is $O\left(NM_T^{3.5}\right)$[25, 26]. $\boldsymbol{v}_n^t$ and $\boldsymbol{w}_n^t$ are obtained from problems (25) and (28), respectively, and the computational complexity of both is $O\left(NM_R^3\right)$. Therefore, for each iteration, the computational complexity of SCRAU is $O\left(NM_T^{3.5} + 2NM_R^3\right)$.

2) Convergence Analysis

During the $t-th$ iteration, the WEP is non-increasing when optimizing $\boldsymbol{u}_n$, i.e., $W_l\left(\boldsymbol{u}_n^{t+1}\middle|\boldsymbol{v}_n^t, \boldsymbol{w}_n^t\right) \le W_l\left(\boldsymbol{u}_n^t\middle|\boldsymbol{v}_n^t, \boldsymbol{w}_n^t\right)$; when optimizing $\boldsymbol{v}_n$, the WEP is non-increasing, i.e., $W_l\left(\boldsymbol{u}_n^t\middle|\boldsymbol{v}_n^t, \boldsymbol{w}_n^t\right) \le W_l\left(\boldsymbol{v}_n^{t+1}\middle|\boldsymbol{u}_n^{t+1}, \boldsymbol{w}_n^t\right)$; since $\boldsymbol{w}_n$ is not an independent variable of WEP when $\boldsymbol{u}_n$ and $\boldsymbol{v}_n$ are fixed, then $W_l\left(\boldsymbol{w}_n^{t+1}\middle|\boldsymbol{u}_n^{t+1}, \boldsymbol{v}_n^{t+1}\right) = W_l\left(\boldsymbol{v}_n^{t+1}\middle|\boldsymbol{u}_n^{t+1}, \boldsymbol{w}_n^t\right)$. Thus, it can be obtained that $W_l(\boldsymbol{u}_n, \boldsymbol{v}_n, \boldsymbol{w}_n)$ is non-increasing during the iteration process, i.e., $W_l\left(\boldsymbol{u}_n^{t+1}, \boldsymbol{v}_n^{t+1}, \boldsymbol{w}_n^{t+1}\right) \le W_l\left(\boldsymbol{u}_n^t, \boldsymbol{v}_n^t, \boldsymbol{w}_n^t\right)$.

Algorithm 1: Sub-problems convex relaxation alternating update (SCRAU) algorithm

Inputs: $M_T, M_{R,c}, M_{R,r}, \omega_0, \omega_1, \partial, \partial^*, \vartheta_0, \vartheta_1, N, P_{tot}, {\sigma_{r,n}}^2, {\sigma_{c,n}}^2, {\sigma_{0,n}}^2, {\sigma_{1,n}}^2, {\sigma_{b,0,n}}^2, {\sigma_{b,1,n}}^2, \Re,$ $\boldsymbol{d}_{\ell,n}, L, \delta_p, \varepsilon$.

Outputs: WEP and power allocation scheme $\left\{\|u_1\|^2, \|u_2\|^2, \|u_3\|^2, ..., \|u_n\|^2\right\}$ in problem (7).

Initialization: $\left\{\boldsymbol{u}_n^{\,0}\right\}, \left\{\boldsymbol{v}_n^{\,0}\right\}, \left\{\boldsymbol{w}_n^{\,0}\right\}$ and iteration index t.

while $\left\|W_l^{t+1}\left(\boldsymbol{u}_n, \boldsymbol{v}_n, \boldsymbol{w}_n\right) - W_l^t\left(\boldsymbol{u}_n, \boldsymbol{v}_n, \boldsymbol{w}_n\right)\right\| \le \varepsilon$ is not satisfied **do**

Solve the convex problem (23) to get $\left\{\boldsymbol{u}_n^{\,t+1}\right\}$ and $\left\{\|u_1\|^2, \|u_2\|^2, \|u_3\|^2, ..., \|u_n\|^2\right\}$;

Solve the MVDR beamforming problem (25) to get the closed-form solutions $\left\{\boldsymbol{v}_n^{\,t+1}\right\}$;

Solve the MVDR beamforming problem (28) to get the closed-form solutions $\left\{\boldsymbol{w}_n^{\,t+1}\right\}$;

$t = t + 1$

end

Figure 2 illustrates the relationship between WEP and the number of iterations for the SCRAU algorithm under various radar SINR values and transmit power conditions. In Fig. 2, with an increasing number of iterations, WEP stabilizes at a fixed value in all three cases. According to the monotonic convergence theorem, the SCRAU algorithm proposed in this paper is convergent [27].

4 Simulation results and analysis

The efficacy of the SCRAU algorithm is verified through simulation in this section. The simulation scenario is shown in Fig. 3. Assume that there is an interference source, the target and the interference source are located at angles $\omega_0 = 0°$ and $\omega_1 = 60°$, respectively. Assume that the number of the total subcarriers is $N = 16$, the numbers of transmitting and receiving elements are $M_T = M_{R,c} = M_{R,r} = 16$. The communication receiving array is located at angle $\partial = 40°$, and $L = 2$ types of sidelobe are pre-designed, i.e., -20 dB and -25 dB. From the perspective of the communication receiving array, it receives desired signals from the communication arrival angle $\partial^* = 0°$ and interference signals from angles $\vartheta_0 = 50°$ and $\vartheta_1 = 70°$. Without loss of generality, we assume a noise variance of 1 for both radar and communication, i.e., $\sigma_{r,n}^2 = \sigma_{c,n}^2 = 1$. All other channel coefficients are set to 0.01, i.e., $\sigma_{a,0,n}^2 = \sigma_{a,j,n}^2 = \sigma_{b,0,n}^2 = \sigma_{b,1,n}^2 = 0.01$, meanwhile, the variance of the communication channel coefficients is set to 1, i.e.,$\sigma_{\gamma,n}^2 = 1$. Assume sufficient frequency spacing between shared subcarriers for independence of observation noise and signal reflections. The iteration stopping constant is set as $\varepsilon = 10^{-5}$.

To better understand the intensity distribution of the transmitted signal in different directions, Fig. 4 shows the relationship between the normalized transmit power

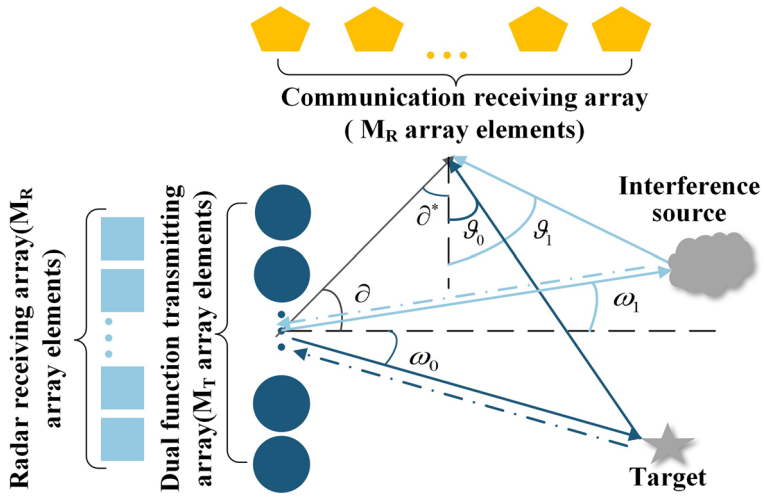

Fig. 3 Simulation scenario of DFRC integrated system

distribution patterns and spatial angles for $L = 2$ transmit beam patterns. Figure 4 shows that the two transmit beams have the same amplitude of the main lobe, this implies that these two beams have comparable detection ranges. The angle of the communication receiving array is $\partial = 40°$, and the communication SLLs are -20 dB and -25 dB, respectively. During the pulse duration, the communication receiving array determines the corresponding communication symbol by comparing the amplitude of received signal from the side-lope during the pulse duration. In addition, the presence of a deep null at azimuth $\omega_1 = 60°$, this means that the system can effectively suppress or minimize interference from that direction, thus improving the system's performance and immunity to interference (Table 1).

Figure 5 shows the communication receiving beam when the main lobe direction is $\partial^* = 0°$, and the interference source direction is located in $\vartheta_0 = 50°$ and $\vartheta_1 = 70°$. From Fig. 5, it can be seen that there are deep nulls in both azimuths $\vartheta_0 = 50°$ and $\vartheta_1 = 70°$. This shows that the proposed algorithm can reduce the beamforming of interference, so that it has less impact on communication. The direction diagram of the communication receive beam is mainly determined by the azimuths ∂^*,ϑ_0 and ϑ_1.

In order to further delve into the power allocation algorithm of beamforming-based DFRC integrated system, we investigate the adaptive power allocation of all N subcarriers under specific channel conditions. A traditional communication system (TCS) without considering the radar SINR constraint and WEP minimization is used as a comparison simulation to verify the performance of the DFRC integrated system. Assuming the state of the communication channel is predetermined. The normalized communication signal-to-noise ratio (SNR) [12, 28] is as shown in Fig. 6a, i.e., $10\log_{10}\left(\sigma_{\gamma,n}^2/\sigma_{c,n}^2\right)$, where it can be seen that subcarriers 2 and 9 are favorable to the communication system. Figure 6b shows the channel strength of the desired radar signal, i.e., $10\log_{10}\left(\sigma_{a,0,n}^2/\sigma_{r,n}^2\right)$; Fig. 6c shows the channel strength of the radar interference signal, i.e., $10\log_{10}\left(\sigma_{a,j,n}^2/\sigma_{r,n}^2\right)$, where subcarriers 3, 4 and 5 interfere more

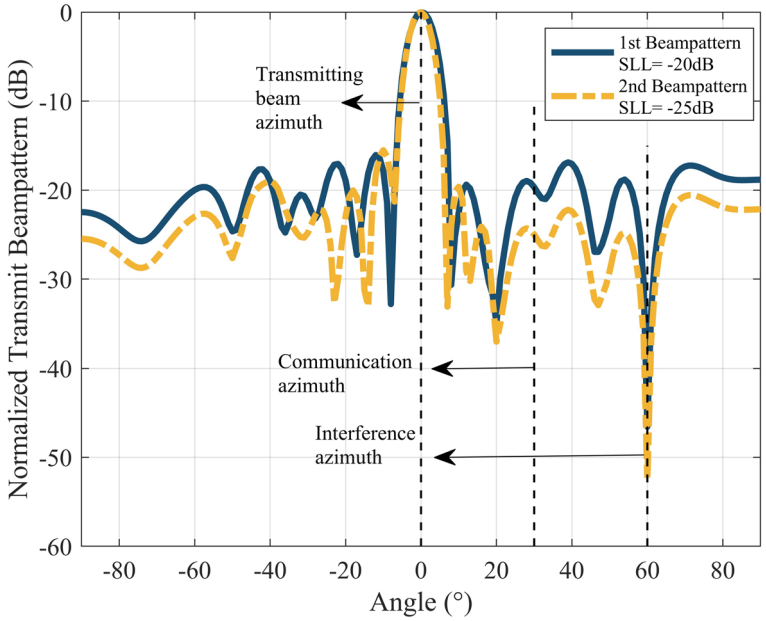

Fig. 4 Transmitting beams in two communication directions have sidelobe levels (SLL) of -20 dB and -25 dB, respectively

Table 1 Parameter values

Parameter	Value	Parameter	Value	Parameter	Value
M_T	16	∂^*	0°	$\sigma^2_{a,0,n}$	0.01
$M_{R,r}$	16	∂	40°	$\sigma^2_{a,l,n}$	0.01
$M_{R,c}$	16	N	16	$\sigma^2_{b,0,n}$	0.01
ϑ_0	50°	L	2	$\sigma^2_{b,1,n}$	0.01
ϑ_1	70°	ω_0	0°	$\sigma^2_{r,n}$	1
SLL_1	−20 dB	ω_1	60°	$\sigma^2_{c,n}$	1
SLL_2	−25 dB	J	1	$\sigma^2_{\gamma,n}$	1

strongly with the radar; Fig. 6d shows the channel strength of the communication interference signal, i.e., $10\log_{10}\left(\sigma^2_{b,1,n}/\sigma^2_{c,n}\right)$.

Figure 7 illustrates the multi-carrier waveform power allocation for the DFRC integrated system under TCS, SINR = 5, and SINR = 10 for the specific channel states described in Fig. 6. When $\delta_p = 2.5$, the power allocation results of $P_{tot} = 10kw$ and $P_{tot} = 30kw$ are shown in Fig. 7a and b, respectively. It is evident from Fig. 7a and b that, in the case of TCS, the highest power allocation is assigned to subcarrier 2. This is because the TCS only considers the communication channel state and does not consider radar SINR constraints. With radar SINR constraints, the DFRC integrated system considers both radar and communication system channel conditions. When the SINR = 10, the subcarrier 9 is allocated with the most power because the subcarrier 9 has the worst radar channel state and communication channel is better, thus more power is needed to meet the constraint of SINR = 10. In addition, higher radar SINR requirements result in a more 'uniform' power allocation across subcarriers.

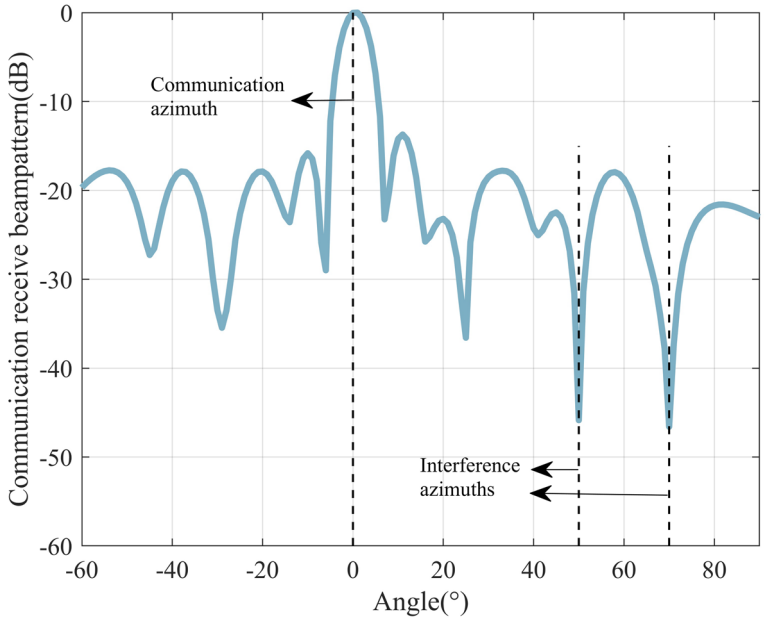

Fig. 5 Receive beampattern of communication

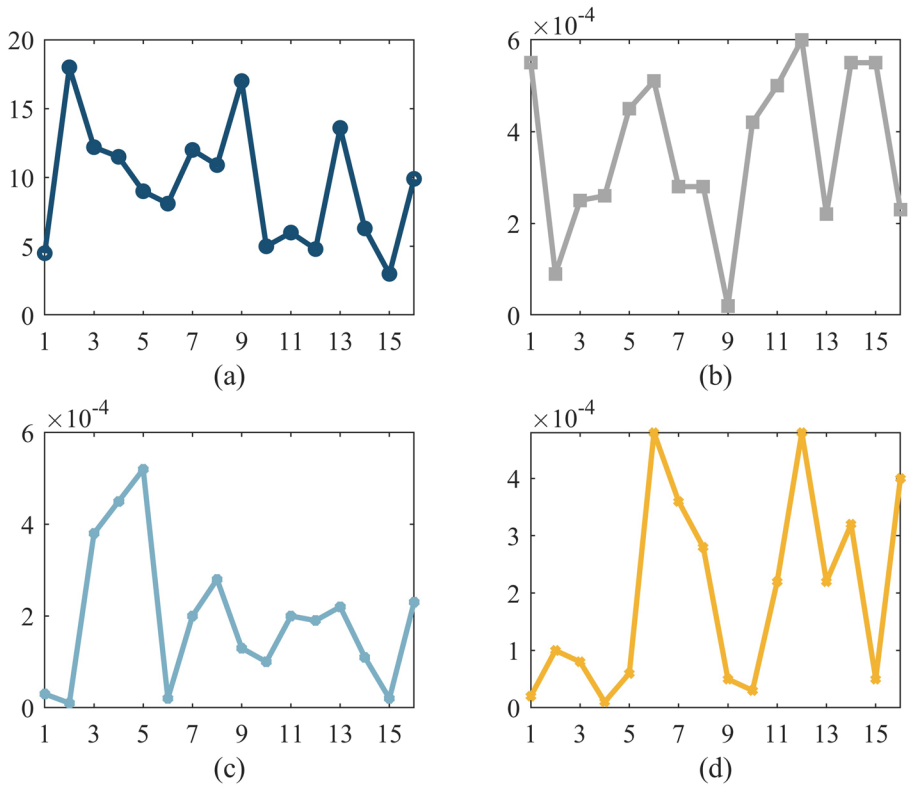

Fig. 6 Channel status of *N* subcarriers. **a** communication channel status, **b** radar channel status, **c** radar interference channel status, **d** communication interference channel status

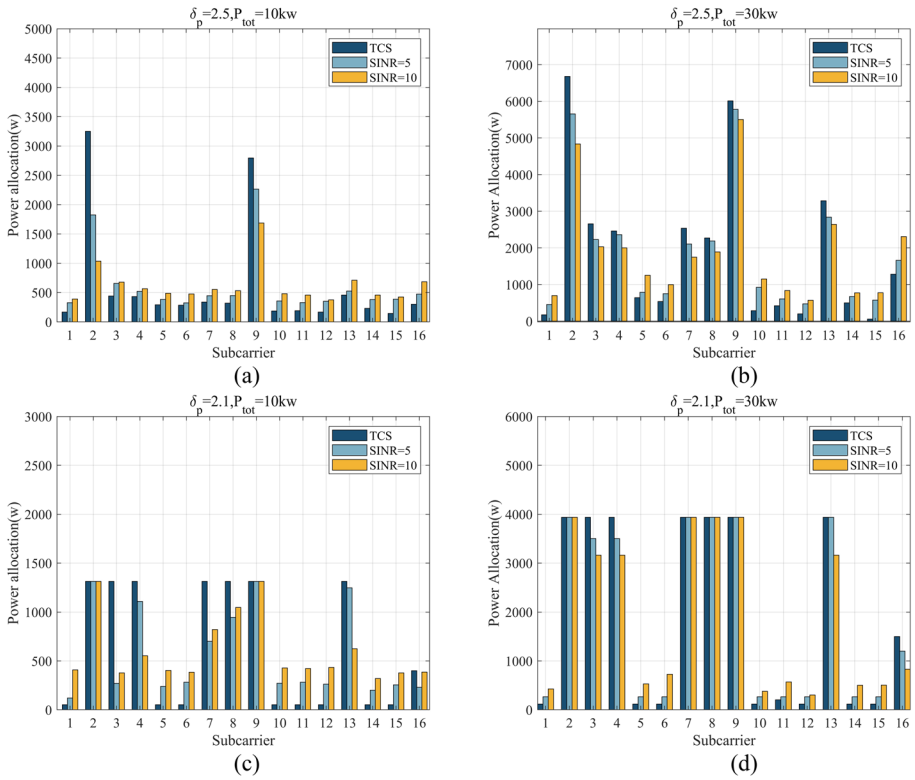

Fig. 7 Power allocation results for TCS, SINR = 5 and 10. **a** $\delta_p = 2.5$, $P_{tot} = 10$ kw, **b** $\delta_p = 2.5, P_{tot} = 30$ kw, **c** $\delta_p = 2.1$, $P_{tot} = 10$ kw, **d** $\delta_p = 2.1$, $P_{tot} = 30$ kw

In general, under low radar SINR, the allocation of power to subcarriers is predominantly influenced by the communication channel state. Conversely, under high radar SINR constrains, the subcarrier power allocation is more significantly impacted by the radar channel state. By comparing Fig. 7a and b, it is clear that increasing total transmitted power leads to a reduction in power allocation discrepancies between the three scenarios. Analysis of Fig. 7a and c shows that when the PAPR constraint is lower, the gap in the distribution of the transmit power over each subcarrier is smaller. In addition, from the deep nulls in Figs. 4 and 5, it is evident that the interference channel states of radar and communication have almost negligible effects on the power allocation.

The proposed SCRAU algorithm is founded upon the sidelobe control information embedding scheme. To validate the efficacy of the SCRAU algorithm, this study compares its performance with that of the QAM-IE algorithm. The QAM-IE algorithm solution process is detailed in [29]. The fundamental principle of the QAM-IE algorithm is to control the amplitude and phase of the sidelobe directed toward the communication user while preserving the main lobe gain of the radar. The communication receiver demodulates the received signals to determine the corresponding communication symbols.

WEP performance of SCRAU and QAM-IE for $\delta_p = 2.5$ with TCS, radar SINR = 5 and 10 is shown in Fig. 8. Figure 8 show that TCS achieves the lowest WEP in both SCRAU and QAM-IE algorithms. TCS, not considering radar performance, allocates transmit power based on communication channel conditions to minimize WEP. From Fig. 8, it is evident that an increase in SINR corresponds to an elevated value of WEP, i.e., the

performance of communication accuracy decreases. Increasing the total transmit power leads to a gradual decrease in WEP under the three conditions. This indicates that a judicious increase in transmit power can effectively reduce WEP, enhancing the reliability of communication transmission. Figure 8 show that the SCRAU algorithm, with the same and transmit power and radar SINR, outperforms the QAM-IE algorithm in combating noise, resulting in a significantly improved WEP performance.

The WEP performance of SCRAU and QAM-IE for radar SINR = 10 with $\delta_p = 2.5$ and $\delta_p = 2.1$ is visualized in Fig. 9. It is clear from Fig. 9 that the increase in total transmitted power is associated with a decrease in WEP. When $\delta_p = 2.5$, the performance of WEP is better. This is due to the fact that the over-restriction on PAPR allows for a more uniform allocation of subcarrier power in specific channel states as shown in Fig. 7. This restriction prevents the DFRC system from adequately considering and accurately achieving the goal of minimizing the communication WEP, which leads to an increase in the WEP. In all cases, the WEP values obtained by the SCRAU algorithm are lower than those of the QAM-IE algorithm. The reason for this difference is that the SCRAU algorithm performs adaptive power allocation based on the channel state conditions with the aim of minimizing the communication WEP while meeting the radar performance constraints. The SCRAU algorithm improves the reliability of the communication transmission and ultimately optimizes the overall performance of the DFRC system. On the communication side, reducing the WEP helps to ensure the integrity and accuracy of data transmission. On the other hand, the QAM-IE algorithm uses a single carrier waveform and does not consider the radar communication coupling of the DFRC system.

The realization of this result can be attributed to several key factors: (1) the proposed method, by modulating in specific directions, mitigates interference from other directions, thereby enhancing the system's performance in complex environments; (2) the method in this paper results in higher achievable rates as well as larger distances

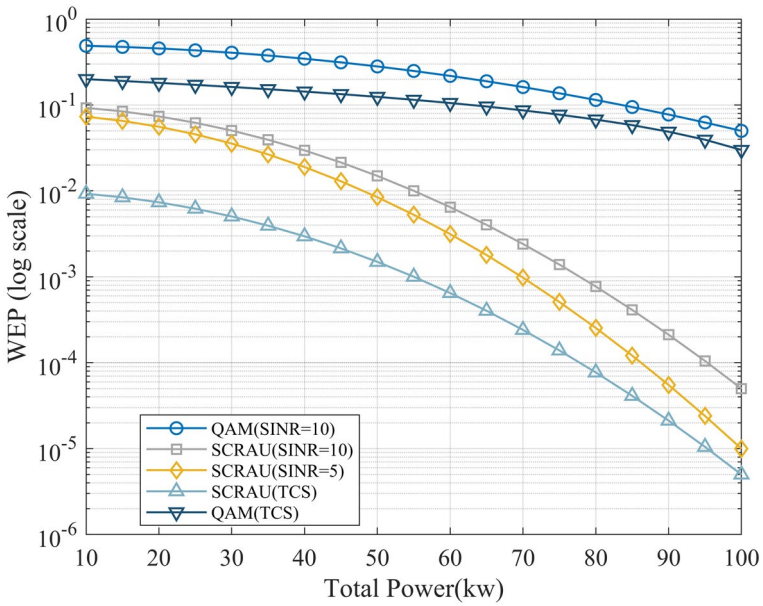

Fig. 8 WEP performance of SCRAU and QAM-IE for $\delta_p = 2.5$ with TCS, radar SINR = 5 and 10

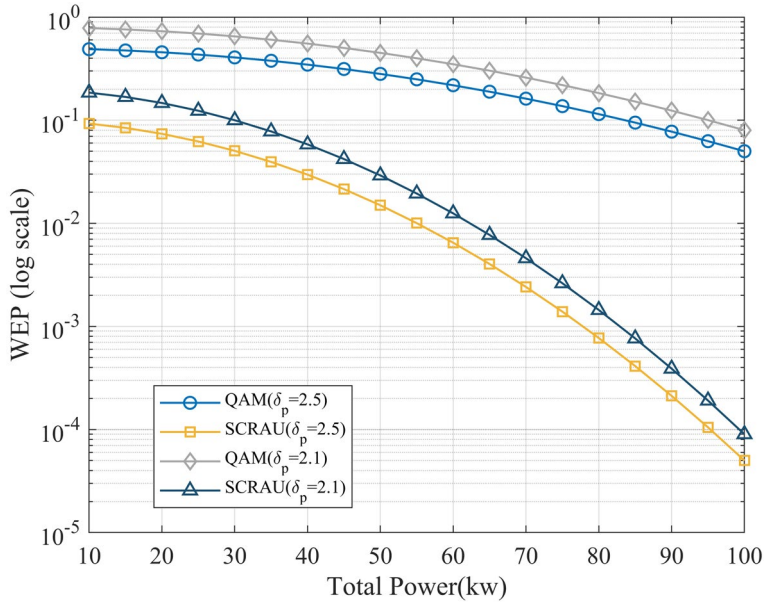

Fig. 9 WEP performance of SCRAU and QAM-IE for radar SINR = 10 with $\delta_p = 2.5$ and $\delta_p = 2.1$

between symbols in the symbol space on the subcarriers, which reduces the communication word error rate; (3) the modulation method in this paper is easier to integrate with the radar system for radar and communication integration; (4) QAM-IE optimizes only the transmit beamforming vectors while higher gain is obtained by optimizing the transmit and receive beamforming vectors; (5) the SCRAU algorithm adaptively allocates power according to the specific channel state.

5 Conclusion

This paper thoroughly investigates the adaptive power allocation problem in dual-functional radar-communication (DFRC) systems. We formulate the optimization criterion as a minimization of word error probability (WEP) under constraints of radar signal-to-interference-noise ratio (SINR), total transmit power, peak-to-average power ratio (PAPR), and sidelobe information. To address the non-convex nature of this problem, we introduce the subproblem convex relaxation alternating update (SCRAU) algorithm, which decomposes the original problem into three sub-problems: (1) dual-function transmit beamforming vector optimization subproblem; (2) design of the radar receive beamforming vector; and (3) design of the communication receive beamforming vector. We prove the decrease and boundedness of WEP, ensuring the convergence of the algorithm. Finally, we compare the SCRAU algorithm with the quadrature amplitude modulation information embedding (QAM-IE) algorithm under various radar SINR, total transmit power, and PAPR conditions. Numerical results demonstrate that the SCRAU algorithm effectively improves WEP performance, enabling adaptive power allocation by jointly considering radar and communication channel states.

A future research direction to consider: in our simulations and analyses, the power limit is set to be fixed within a single pulse duration. Future work will further explore optimization strategies for power allocation under different PRI conditions to ensure system performance under various operating conditions.

Author contributions
Each author made a significant contribution to the article. JT was responsible for the simulation design and implementation and the original draft of the article. ZK Z participated in the simulation design and review and revision of the article. All authors reviewed and approved the final version of the article.

Funding
This work was supported by the National Natural Science Foundation of China under Grant Nots. 61871203.

Availability of data and materials
Not applicable.

Declarations

Ethics approval and consent to participate
All procedures performed in this paper were in accordance with the ethical standards of research community.

Competing interests
We declare that we have no financial and personal relationships with other people or organizations that can inappropriately influence our work and there is no professional or other personal interest of any nature or kind in any product, service and/or company that could be construed as influencing the position presented in or the review of the manuscript entitled.

Received: 29 February 2024 Accepted: 16 September 2024
Published online: 29 September 2024

References

1. L. Zheng, M. Lops, Y.C. Eldar, X. Wang, Radar and communication coexistence: an overview: a review of recent methods. IEEE Signal Process. Mag. **36**, 85–99 (2019). https://doi.org/10.1109/MSP.2019.2907329
2. S.K. Agrawal, A. Samant, S.K. Yadav, Spectrum sensing in cognitive radio networks and metacognition for dynamic spectrum sharing between radar and communication system: a review. Phys. Commun. **52**, 101673 (2020). https://doi.org/10.1016/j.phycom.2022.101673
3. C. Shi, Y. Wang, F. Wang, S. Salous, J. Zhou, Joint optimization scheme for subcarrier selection and power allocation in multicarrier dual-function radar-communication system. IEEE Syst. J. **15**, 947–958 (2020). https://doi.org/10.1109/JSYST.2020.2984637
4. L. Chen, Z. Wang, Y. Du, Y. Chen, F.R. Yu, Generalized transceiver beamforming for DFRC with MIMO radar and MU-MIMO communication. IEEE J. Sel. Areas Commun. **40**, 1795–1808 (2022). https://doi.org/10.1109/JSAC.2022.3155515
5. J. Zeng, B. Liao, Transmit and receive hybrid beamforming design for OFDM dual-function radar-communication systems. EURASIP J. Adv. Signal Process. **2023**, 37 (2023). https://doi.org/10.1186/s13634-023-00996-2
6. T. Tian, G. Li, H. Deng, J. Lu, Adaptive bit/power allocation with beamforming for dual-function radar-communication. IEEE Wirel. Commun. Lett. **11**, 1186–1190 (2022). https://doi.org/10.1109/LWC.2022.3160674
7. A. Hassanien, M.G. Amin, E. Aboutanios, B. Himed, Dual-function radar communication systems: a solution to the spectrum congestion problem. IEEE Signal Process. Mag. **36**, 115–126 (2019). https://doi.org/10.1109/MSP.2019.2900571
8. A. Hassanien, M.G. Amin, Y.D. Zhang, F. Ahmad, Signaling strategies for dual-function radar communications: an overview. IEEE Aerosp. Electron. Syst. Mag. **31**, 36–45 (2016). https://doi.org/10.1109/MAES.2016.150225
9. A. Hassanien, M.G. Amin, Y.D. Zhang, F. Ahmad, Dual-function radar-communications: information embedding using sidelobe control and waveform diversity. IEEE Trans. Signal Process. **64**, 2168–2181 (2016). https://doi.org/10.1109/TSP.2015.2505667
10. W. Baxter, E. Aboutanios, A. Hassanien, Joint radar and communications for frequency-hopped MIMO systems. IEEE Trans. Signal Process. **70**, 729–742 (2022). https://doi.org/10.1109/TSP.2022.3142909
11. Y. Yao, P. Miao, Z. Chen, Cognitive waveform optimization for phase-modulation-based joint radar-communications system. IEEE Access. **8**, 33276–33288 (2020). https://doi.org/10.1109/ACCESS.2020.2974787
12. T. Tian, T. Zhang, L. Kong, Y. Deng, Transmit/receive beamforming for MIMO-OFDM based dual-function radar and communication. IEEE Trans. Veh. Technol. **70**, 4693–4708 (2021). https://doi.org/10.1109/TVT.2021.3072094
13. Y. Yang, J. Mei, D. Hu et al., Research on reducing PAPR of QAM-OFDM radar-communication integration sharing signal. J Eng **2019**, 8042–8046 (2019). https://doi.org/10.1049/joe.2019.0726
14. Y. Huang, S. Hu, S. Ma, Z. Liu, M. Xiao, Designing low-PAPR waveform for OFDM-based RadCom systems. IEEE Trans. Wireless Commun. **21**, 6979–6993 (2022). https://doi.org/10.1109/TWC.2022.3153606

15. Z. Li, J. Xie, H. Zhang, J. Ge, C. Qi, A robust power allocation strategy based on benefit–cost ratio for multiple target guidance in the C-MIMO radar system under blanket jamming. EURASIP J. Adv. Signal Process. **2022**, 48 (2022). https://doi.org/10.1186/s13634-022-00880-5
16. C. Shi, S. Salous, F. Wang, J. Zhou, Low probability of intercept-based adaptive radar waveform optimization in signal-dependent clutter for joint radar and cellular communication systems. EURASIP J. Adv. Signal Process. **2016**, 111 (2016). https://doi.org/10.1186/s13634-016-0411-6
17. J.G. Proakis, *Digital communications*, 4th edn. (McGraw Hill, New York USA, 2001), p.444
18. A.D. Maio, Y. Huang, M. Piezzo, S. Zhang, A. Farina, Design of optimized radar codes with a peak to average power ratio constraint. IEEE Trans. Signal Process. **59**, 2683–2697 (2011). https://doi.org/10.1109/TSP.2011.2128313
19. Z. Cheng, Z. He, B. Liao, M. Fang, MIMO radar waveform design with PAPR and similarity constraints. IEEE Trans. Signal Process. **66**, 968–981 (2017). https://doi.org/10.1109/TSP.2017.2780052
20. A. Tkacenko, P.P. Vaidyanathan, Iterative greedy algorithm for solving the FIR paraunitary approximation problem. IEEE Trans. Signal Process. **54**, 146–160 (2005). https://doi.org/10.1109/TSP.2005.861054
21. M.N. Omidvar, M. Yang, Y. Mei, X. Li, X. Yao, DG2: a faster and more accurate differential grouping for large-scale black-box optimization. IEEE Trans. Evol. Comput. **21**, 929–942 (2017). https://doi.org/10.1109/TEVC.2017.2694221
22. Y. Sun, P. Babu, D.P. Palomar, Majorization-minimization algorithms in signal processing, communications, and machine learning. IEEE Trans. Signal Process. **65**, 794–816 (2016). https://doi.org/10.1109/TSP.2016.2601299
23. M. Grant, S. Boyd, CVX: matlab software for disciplined convex programming, version 2.1. (2014). Accessed 28 Feb 2024. http://cvxr.com/cvx
24. J. Capon, High-resolution frequency-wavenumber spectrum analysis. Proc. IEEE **57**, 1408–1418 (1969). https://doi.org/10.1109/PROC.1969.7278
25. X. Yu, K. Alhujaili, G. Cui, V. Monga, MIMO radar waveform design in the presence of multiple targets and practical constraints. IEEE Trans. Signal Process. **68**, 1974–1989 (2020). https://doi.org/10.1109/TSP.2020.2979602
26. Z. Cheng, B. Liao, Z. He, J. Li, J. Xie, Joint design of the transmit and receive beamforming in MIMO radar systems. IEEE Trans. Veh. Technol. **68**, 7919–7930 (2019). https://doi.org/10.1109/TVT.2019.2927045
27. A. Aubry, A. DeMaio, A. Farina, M. Wicks, Knowledge-aided (potentially cognitive) transmit signal and receive filter design in signal-dependent clutter. IEEE Trans. Aerosp. Electron. Syst. **49**, 93–117 (2013). https://doi.org/10.1109/TAES.2013.6404093
28. F. Wang, H. Li, M.A. Govoni, Power allocation and co-design of multicarrier communication and radar systems for spectral coexistence. IEEE Trans. Signal Process. **67**, 3818–3831 (2019). https://doi.org/10.1109/TSP.2019.2920598
29. A. Ahmed, Y.D. Zhang, Y. Gu, Dual-function radar-communications using QAM-based sidelobe modulation. Digital Signal Process. **82**, 166–174 (2018). https://doi.org/10.1016/j.dsp.2018.06.018

Publisher's Note